Int J Mech Mater Des (2006) 3:223–236
DOI 10.1007/s10999-007-9026-2

Position control of an experimental robotic arm driven by artificial muscles based on shape memory alloys

Cedric Cocaud · Aaron Price · Amor Jnifene · Hani Naguib

Received: 29 November 2006 / Accepted: 21 March 2007 / Published online: 23 May 2007

Abstract This paper presents a study on the potential application of artificial muscles based on shape memory alloys as linear robotic actuators. An extended discussion on various control techniques and ways of biologically inspired muscle arrangements is presented. A two DOF experimental robotic arm was built and used to test the performance of the proposed artificial muscle configurations, and a biologically inspired control strategy using a rule-base concept was developed and tested using the two DOF experimental robotic arm.

Keywords Shape memory alloys · Artificial muscles · Rule-based control · Robotic arm

C. Cocaud · A. Price
Mechanical Engineering, University of Ottawa, Ottawa, ON, Canada

A. Jnifene (✉)
Mechanical Engineering, Royal Military College of Canada, Station Forces, PO Box 17000, Kingston, ON, CanadaK7K 7B4
e-mail: amor.jnifene@rmc.ca

H. Naguib
Mechanical Engineering, University of Toronto, Toronto, ON, Canada

1 Introduction

A considerable portion of the population relies on prosthetic devices to overcome the difficulties associated with the loss of a limb through congenital defects, trauma, or disease. It has been reported that 200–500 major amputations are performed per million people each year (Dormandy et al. 2004). Modern actuated prostheses are commonly powered by electric servomotors. While achieving reasonable kinematic performance, they are typically heavy and bulky (Pfeiffer et al. 1999). Because of these limitations, most users tend to substitute these types of prosthesis by older (but lighter) manually activated prostheses. A recent survey on patient's satisfaction with prosthetic devices indicated that 22.9% were dissatisfied with the weight of their prosthetic limb (Pezzin 2004). Thus, there is a clear need for practical prosthetic devices that combine both, automatic actuation and light weight structure.

In an attempt to solve this problem, several alternative lightweight actuators used as artificial muscles (AMs) have been investigated. These AMs include electroactive polymers (EAP) and pneumatic muscles (Bar-Cohen et al. 1998; Chou and Hannaford 1996). The actuation force generated by EAP based artificial muscles is too low to be of any practical use at the present state of development. Pneumatic muscles require a bulky set of pneumatic system to supply and control the flow of compressed gas needed to allow these muscles to produce useful work. A vast

amount of research has been reported on the application of shape memory alloy (SMA) as artificial muscles in both straight tensile (Pfeiffer et al. 1999; Makaran et al. 1993; De Laurentis and Mavroidis 2002; Gorbet and Russell 1995) and hybrid composite (Barrett and Gross 1996; Icardi 2001) configurations with promising results. The first configuration results in actuators which produce high force and low strain, while the second configuration typically results in actuators that produce high strains and low force.

Different control schemes have been reported in the literature. Time delay control (TDC) was compared to PID and relay control (RC) in (Jik Lee and Ju Lee 2004), the latter corresponding to the so called ''bang–bang'' or on-off control scheme. Results showed the inadequacy of the PID control scheme when using gains based on the Ziegler-Nichols tuning method. This result showed that the highly nonlinear response of the SMA (i.e. hysteresis, saturation, shape memory effects, etc.) could not be approximated as a first order time delay system for control purposes. TDC and RC control seemed to give satisfactory results with similar time response. Although RC control gave the fastest response, it could not avoid the limit-cycle problem during the steady state response of the actuator, resulting in small high-frequency oscillations around the desired value. In an attempt to improve the energy efficiency of electrical resistance actuation of SMA actuators using the RC control scheme, pulse width (PW) modulation and pulse width pulse frequency (PWPF) modulation were tested and compared to a continuous PD controller (Ma and Song 2003). Great energy savings and enhanced robustness to external disturbances could be achieved with the PW modulator while the control accuracy observed was superior to the other controllers.

More complex control schemes such as neural network (NN) and Fuzzy logic (Tu et al. 1999) where tested, including a combination of NN controller for hysteresis compensation and sliding-mode based robust controller to ensure stability and robustness toward nonlinearities and disturbances (Song et al. 2003). This hybrid controller was tested by using a sinusoidal test signal with a period of 60 s (a typical timeframe for allowing SMA to complete a full activation–relaxation cycle). Results showed that the SMA wire used for testing accurately followed the control signal with a maximum error of 2%. Although this controller seems to give impressive results, it must be mentioned that other forms of SMA such as ribbon or thin sheets presents increased nonlinearities that may not be as easily compensated. Other approaches have been pursued to solve the problem of compensating for SMA nonlinearities. Offline system linearization has been attempted using theoretical models to predict static hysteresis, but open-loop compensation can generate significant artificial disturbances at the controller level if discrepancies exist between the model and the actual response. Thus, offline linearization usually lacks the robustness required for general SMA based applications. Adaptive control schemes that do both identification and hysteresis compensation have been developed using the KP hysteresis model under constant loads (Webb et al. 1998) and under varying loads (Webb et al. 1999). This model represents the hysteretic dependence of SMA wire output on the temperature. The output is given as an infinite sum of weighted simple hysteresis operators. Experimental results conducted on SMA wires showed that the adaptive model was able to account for variations in hysteresis caused by changes in loading conditions. The KP-based controller demonstrated excellent tracking abilities for continuous signals of up to 20 Hz, while PI output-error feedback control method failed at 4 Hz. Most controllers, including the ones discussed earlier, base their error dynamic on displacement. Theoretically, the temperature could also be used in a feedback control to regulate the amount of activation of the SMA. In practice, temperature is very hard to measure and most of the time a state estimator (Elahinia et al. 2004) or a constitutive model (Jik Lee and Ju Lee 2004; van der Wijst et al. 1997; Garner et al. 2000) are used when temperature is included in the control scheme. Usually, temperature control cannot be implemented alone for position control. Its major drawback is that small perturbations can produce large variations on the output position. Position and temperature feedback have been combined in a dual stage controller based on a PI combined with a low pass filter (Troisfontaine et al. 1997). Experimental results showed a satisfactory response for input signal tracking using a sinusoidal command signal of 0.1 Hz. Interesting results have also been obtained for force and position control based on a mathematical model that can capture the

non-linear behaviour of SMA through experimental identification techniques for the material properties (Benzaoui et al. 1999). The mathematical model is based on the Helmholtz free energy expression and takes into account the individual contribution of strain, temperature, stress induced martensite volume fraction and temperature induced martensite volume fraction. This dynamic non-linear model is used with a control law based on the Lie algebra.

Following this brief review of control schemes for SMAs and SMA based actuators, it is worth mentioning that the RC control (or bang–bang controller) is very similar to the method of activation of human skeletal muscles (McComas 1996). The motorneurons responsible for sending the control signal to the muscle are frequency based and the output is a voltage of constant amplitude. Emphasizing the energy savings demonstrated by PW modulation (Ma and Song 2003) and the ease of implementing the RC control scheme as well as its good performances (Jik Lee and Ju Lee 2004), the biomimetic approach seems to have great potential for online control of structures equipped with several SMA based actuators. Following this biomimetic approach, this paper presents a control scheme aiming to regulate the displacement of a single artificial muscle and to coordinate several artificial muscles in order to achieve a particular motion using a prosthetic arm.

2 SMA based actuator

SMA have been commonly used in straight tension for actuation purposes, which limited their maximum strain capabilities to 4–6%. Although significantly greater than other inert metal materials, this strain remains too small for applications such as man-size robots. Hybrid composites such as the super active shape memory alloy composite (SASMAC) (Barrett and Gross 1996) were found to produce much greater strains and extended the range of applications where SMA can be used. The key concept that allows strain capabilities greater than 6% is to use the SMA in a pattern that can achieve greater global strain while limiting local strain to the maximum capabilities of the material. The SASMAC can achieve strain ranging from 10 to 20%. The work presented in this paper follows the development of an actuator that uses a pattern allowing much greater strain, ranging from 30 to 40%. This improvement was based on increasing the SMA wire section (i.e. using ribbon instead of wires), braiding several strands together, and using the pattern depicted in Fig. 1.

Fig. 1 SMA artificial muscle

The ribbon is characterized by an enhanced elasticity and strain capabilities over conventional SMA wires (13% strain for the ribbon against $4 \sim 5\%$ strain for a typical Flexinol SMA wire). Braiding several strands together increases local elasticity while increasing the global actuation force of the actuator. The *figure 8 pattern* allows restricting local strain below the limits of the ribbon, while achieving an overall linear strain of up to 37% in average. Depending on the loading conditions, the maximum strain may decrease up to the point where the external force overcomes the internal actuation force generated within the SMA actuator. Significant linear displacement can still be achieved under a load of up to 0.4 kg. All the information about the dimension, stress–strain curves, and the phase transformation characteristic of the SMA wires used in this study can be found in (Price et al. 2007) nwhich deals specifically with the thermo-mechanical properties of the proposed SMA base artificial muscles.

3 Experimental set-up

Figure 2 shows a schematic representation of the experimental set-up that was used to carry on the research presented in this paper. The overall system consists of an elbow joint driven by two SMA based artificial muscles. The amount of power required to activate the two artificial muscles cannot be supplied directly from the I/O control board. Thus, two MOSFET power transistors are used as power amplifiers and to ensure that no power is supplied to the artificial muscle during the relaxation phase. Using pulse modulated servo-amplifiers proved to be unsatisfactory in achieving this goal. When the control signal is set to zero, the small output power

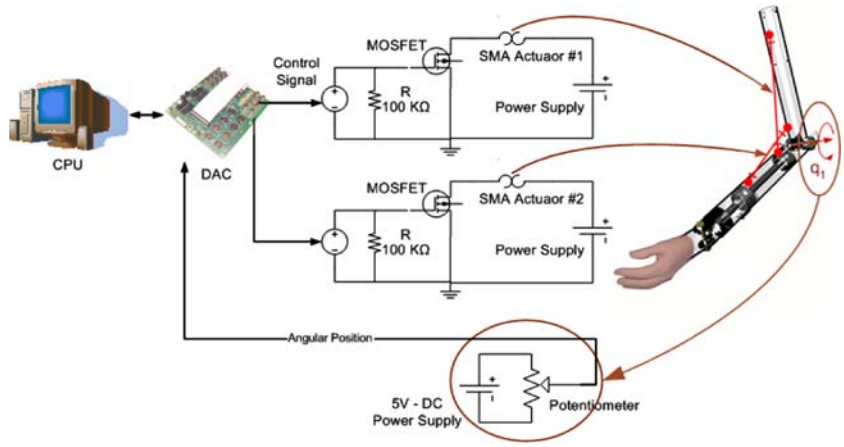

Fig. 2 Experimental setup for arm control

oscillations of the pulse modulated servo amplifier around the zero value, combined with the very small electric load of the circuit, were enough to create a residual current prohibiting any relaxation of the artificial muscle.

The control board is the Q8 from Quanser and featuring 8 analog inputs, 8 analog outputs, and 8 encoder inputs. Two of the 8 analog outputs are used to activate the two artificial muscles. The angular position of the elbow joint is measured using a rotary potentiometer. The signal from the potentiometer is fed to the control board through one of the 8 analog inputs. The control system is implemented using Matlab/Simulink and the Real Time Workshop (RTW) from Mathworks and WinCon 4.1 from Quanser.

In the first part of the experimentation, a single artificial muscle attached to a slider mechanism is activated in order to investigate its behaviour when used with a simple ON/OFF control scheme. The control hardware includes an LVDT sensor providing direct feedback of the linear displacement of the actuator. In the second part of this work, artificial muscles are attached on the arm as shown in Fig. 2 and activated using different control schemes.

4 Control of SMA based artificial muscles

Different control scheme were considered to coordinate groups of AM as well as individual ones. Taking a biomimetic approach to this problem, it was found that biological muscles are controlled by sending small electrical pulses through the motorneurons. The amount and rate of activation of muscles are controlled by the frequency of these pulses rather than their amplitude. Depending on the muscle arrangement, one motorneuron can control one muscle or an entire group of muscles. The first arrangement allows high precision control over the level of activation of the muscle to which that group of fibers belongs. The second arrangement gives no control over individual muscle activation, but can provide high activation forces while requiring very few commands from the controller (the brain and spinal chord in this case). The human anatomy offers different examples of muscular systems to achieve control of both position and actuation force. The most common configurations are the following:

a. Complementary muscles arrangement. This arrangement refers to the combined action of spurt and shunt muscles. The muscles are attached at different points on the skeletal structure around a given joint. Once activated, they all contribute to the same motion. Sequentially activating such muscles can increase the force and/or the rate of motion.

b. Parallel muscles arrangement. In this arrangement, the muscles can be activated all at once to increase the actuation power available. This type of arrangement also serves the purpose of producing a relatively constant actuation force over long period of time. As it is, SMA based artificial muscle cannot contract indefinitely without overheating and losing part of their memory in the process. Thus, every SMA actuator must have enough time to cool down after being activated. The concept is to implement a switch

control scheme that alternatively activates parallel artificial muscles to maintain a certain position under given loading conditions.

c. Muscles in series. This configuration consists of connecting several muscles in series and each muscle can be controlled and activated independently. This configuration provides a way of achieving a more constant force output with better control over linear displacement when considering the entire chain of muscles. However, this approach requires complex control schemes and most importantly, each muscle requires separate power supply and separate strain sensor which makes the whole system costly and potentially bulky at this stage of development. This concept remains an interesting solution that could be investigated in future studies.

During the investigation of the various ways of controlling SMAs without using complex mathematical models, two methods for controlling multiple-muscles configurations were tested and compared. The first one is a simple Bang–Bang controller that activates all muscles at the same time until the desired angular position is reached. The second one consists of a rule based controller that activates each muscle individually depending on the proximity of the arm to the desired angular position. The latter takes into account the error of the angular position as well as the rate of change of that error with respect to time. A detailed description of the rule based controller is presented in the following section.

4.1 Rule-based control of SMA artificial muscles

During a typical limb motion, a human operator can intuitively determine which muscle should be activated without using complex mathematical transforms or any optimization procedures. This intuitive knowledge is the result of years of continuous training. In order to emulate the use such intuitive knowledge, and to avoid the use of any mathematical models of the SMA based artificial muscle, a rule based control system is used in the present study. The rule-based controller is essentially a Fuzzy Logic Controller with rectangular membership functions. The rules that govern the activation of a group of SMA muscles and reproduce human movements are developed and implemented on the experimental set-up shown in Fig. 2.

4.1.1 Rule-based concept

In contrast with other control schemes, the one presented in this paper is not based on the individual strain–stress state of each artificial muscle. The controller is designed to set the activation of each muscle based on the overall configuration of the arm. A configuration is described with two variables; (1) the extension of the arm measured by the angular displacement at the elbow, and (2) the rate at which the forearm is rotating with respect to the upper arm. Based on the current and the desired configurations of the arm, the controller selects the appropriate activation scheme for each muscle. All activation schemes are determined in advance, and each one represents a rule. The set of activation schemes constitute the controller's rule-base. In the present case, there are two artificial muscles representing the brachioradialis and the biceps that actuate the elbow joint. The inputs to the controller are: The error of the elbow's angular position, and the rate of change of the error. Since this work is only concerned with two complementary muscles, the number of possible muscle activations is limited to the following cases: (a) Both muscles are continuously activated and deactivated, and (b) only one muscle is activated at a time. In order to combine the biomimetic control schemes corresponding to the complementary muscles arrangement and the parallel muscle arrangement, three types of activations were considered: (1) all muscles are ON at the same time, maximizing the actuation force as well as the response time, (2) only one of the two muscles is activated at a time, and (3) all muscles are OFF. For type (2), the two muscles are activated alternately in order to allow sustained actuation while avoiding overheating. If the actuation characteristics of the two muscles are not identical, one muscle will actually play the role of the main force provider for motion, while the second one will play the role of stabilizer once the arm is close to the target position. This would occur if the position reached corresponds to the desired one, or in the event of an overshoot, antagonist muscles or gravity would pull the arm back toward the desired position. These three possibilities are identified by the numerical values 0, 1, 2, representing the number of muscles activated during the motion of the arm. 1 means that the muscles are activated one at a time and 0 and 2 represent continuous activation or inactivation of both muscles respectively.

4.1.2 Encoding rule-base's inputs

Similar to the process of fuzzification used in Fuzzy Control, rectangular membership functions (Fig. 3) are used to group sets of similar muscular configurations. The main reason behind using this type of function is that each specific arm configuration requires a particular combination of muscles activated under some predefined sequence.

Since the number of possible muscular activations is discrete and can't be averaged to give intermediate solutions at the limit of two typical situations, the only way to respond appropriately to these limit cases is to carefully define the range of values representing each typical situation. Cases where the input variables fall exactly at the limit between two linguistic values were solved by simply rounding up the input parameter to the worst case (i.e. farthest linguistic value from *ZERO*).

4.1.3 Rule-base implementation

Due to the particular nature of the present application, all techniques using the weighted sum of the certainties are not applicable. Instead, a direct look-up table shown in Table 1 was developed. This table represents all possible situations (i.e. the state of the angular position error and the angular velocity) and the corresponding state of muscular activation required to decrease this error. The general logic behind this look-up table is to minimize the actuation effort as the arm approaches the desired position. It also attempts to reduce the speed of the arm around its final position by decreasing the number of muscles activated at that point.

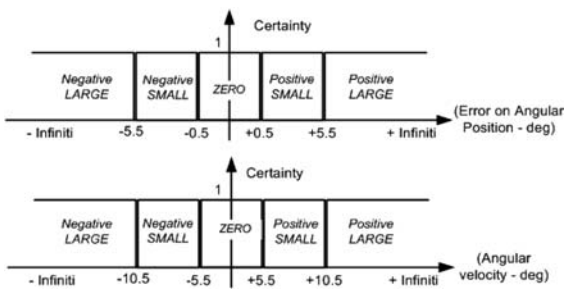

Fig. 3 Rectangular membership functions for input parameters

Using a standard look-up table, the rule selection process would normally have to make a series of comparison to find to which category each input belongs, i.e. one of the five linguistic categories ranging from positive big (PB) to negative big (NB). In order to speed-up this process a mathematical formula was derived to directly evaluate the type of activation scheme ''A'' that the controller should select:

$$A = (\text{angular velocity}) * (\text{angular position error})^2$$

The *angular velocity* and *angular position error* parameters use integer values ranging from 1 to 5, corresponding to the five linguistic values ranging from PB to NB, respectively as indicated in Table 1. Based on this conversion from linguistic to numerical values the equation above gives the following results (Table 2):

Using the value computed in the look-up table shown above, only three comparisons need to be made to determine the activation schemes: If $A < 4$ the activation scheme is (2), If $A \in [5; 17]$ the activation scheme is (1), and If $A > 18$ the activation scheme is (0). In this way, the total number of comparison that must be performed on-line drops from 10 (2 inputs × five categories) to 3. Because the rule base in Table 1 is not symmetric, the angular position error has to be squared

Table 1 Rule base for muscle activation

		Error				
		PB (1)	PS (2)	Z (3)	NS (4)	NB (5)
$\frac{de}{dt}$	PB (1)	(2)	(2)	(1)	(1)	* (0)
	PS (2)	(2)	(1)	(0)	(0)	* (0)
	Z (3)	(2)	(1)	(0)	* (0)	* (0)
	NS (4)	(2)	(1)	(0)	* (0)	* (0)
	NB (5)	(1)	(0)	* (0)	* (0)	* (0)

Table 2 Computed activation values

		Error				
		PB (1)	PS (2)	Z (3)	NS (4)	NB (5)
$\frac{de}{dt}$	PB (1)	1	4	9	16	25
	PS (2)	2	8	18	32	50
	Z (3)	3	12	27	48	75
	NS (4)	4	16	36	64	100
	NB (5)	5	20	45	80	125

such that the ranges of values corresponding to each activation scheme do not overlap.

5 Experimental results

The experimental work described in this paper was carried out in two parts: First, experiments are performed to characterize the actuator response for a single SMA artificial muscle. Second, the control of a two-muscle arrangement attached at the elbow joint of a two DOF robotic arm as shown in Fig. 2 is tested and analyzed. In order to assess the performance of the artificial muscle, the following performance measures are used:

t_0	Time of the first measurable displacement
t_r	Time at which actuator's displacement reaches the desired value
t_{ss}	Time at which actuator's response reaches its steady state
t_h	Time required to reach a temperature above the phase transition temperature of the SMA such that the actuation force generated overcomes external forces that prohibited contraction
t_c	Cooling time required to reach AM initial length (i.e. fully stretched length)
t_p	Length of time where the actuator shows a constant displacement (i.e. plateau type of response) without being activated
$\frac{DD}{MD}$	Ratio of the desired displacement over the maximum displacement reachable by the actuator. This value is a constant for each individual test
$\frac{d}{MD}$	Measure of the actuator's strain (i.e. actual displacement over maximum displacement)
Δt_x	Period of time between activation and characteristic ''x'' (i.e. $\Delta t_x = t_x - t_{act}$). For all tests, $t_{act} = 5$ s

5.1 Single artificial muscle characterization

In order to mimic the activation mechanism of biological muscles, a simple on-off controller was used for this part. This controller corresponds to the so-called Band–Bang controller that activates the muscle until the desired displacement is reached leaving the possibility of overheating the SMA if the process is not carefully monitored. The experimental set-up consists in a slider mechanism to which one end of an SMA actuator is attached while the other end is fixed. A bias spring is attached in series with the SMA, producing the necessary counter force to pull the actuator back when it is not activated (Fig. 4).

The linear displacement of the actuator is measured using an LVDT.

5.1.1 *Artificial muscle response under unloaded conditions*

The first series of tests consisted in measuring the time response and overshoot of the AM when no load was applied. The AM was installed horizontally such that the only force present during activation was the small friction force of the slider mechanism. Four tests have been carried out using different set-points and the time responses are shown in Fig. 5.

The results shown in Table 3 show that Δt_o changes depending on the initial condition of the SMA wire. Since this parameter is a function of the difference between the SMA's initial temperature and phase transition temperature (i.e. a constant defined by the type of SMA used), as well as the heating rate (a function of the power applied) which was held constant for the duration of the tests, the variations of Δt_o can only be caused by the initial temperature of the actuator. Test no. 4 with the largest Δt_o was performed first when the muscle is at room temperature. Test no. 2 and test no. 3 were performed only few minutes apart which means that the muscle did not require a lot of time to heat up resulting in a shorter Δt_o. Table 3 also shows one of the basic characteristics of SMA: the overshoot caused by the rate at which the SMA cools down once the supplied power is set to zero diminishes as DD/MD approaches unity. This is due to the fact that for large desired displacement or set-point, the amount of heat required to produce additional displacement is greater than the thermal energy left in the SMA after the input power is turned off. Conversely, the residual thermal energy for a small set-point exceeds the amount of energy required to maintain the SMA at the desired displacement. Thus, although the SMA is continuously cooling down, the temperature remains high enough to generate additional displacement and causing it to overshoot.

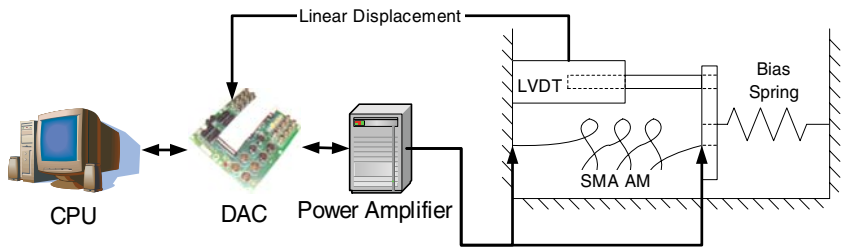

Fig. 4 Experimental set-up for single artificial muscle characterization

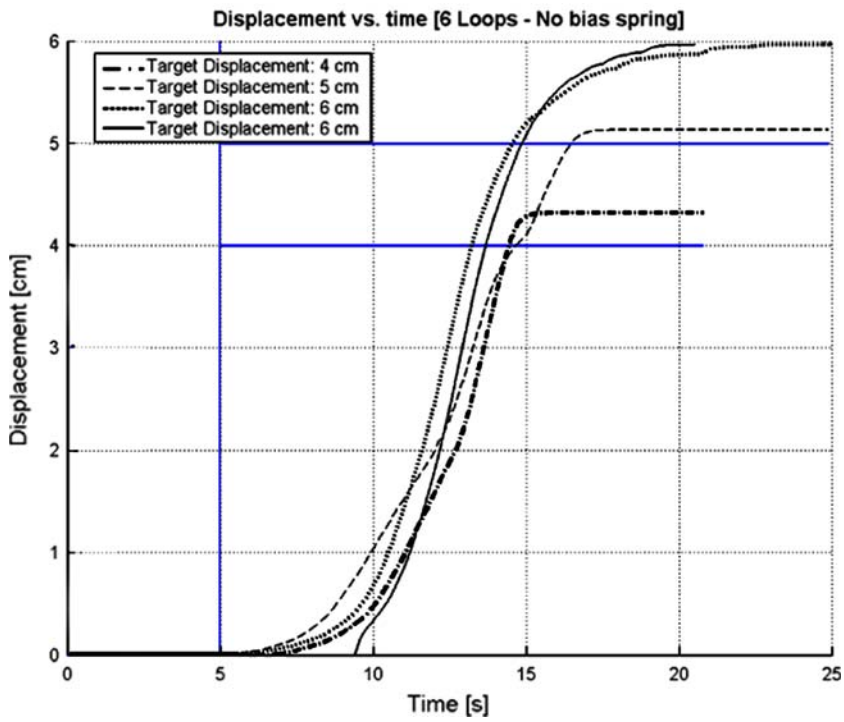

Fig. 5 Displacement of a single SMA muscle under free loading conditions

Table 3 Experimental results—Free loading conditions

Test no.	Set-point	Δt_o	Δt_r	Δt_{ss}	PO	DD/MD
1	4	1.7	9.4	10.5	7%	0.66
2	5	0.5	11.3	12.4	2.3%	0.83
3	6	0.5	17.8	17.8	0%	1
4	6	4.3	14.61	14.61	0%	1

5.1.2 Artificial muscle response using a bias spring

In order to reduce the amount of overshoot, a bias spring needs to be attached in series with the SMA muscle. However, the force generated by the spring has the adverse effect of decreasing the maximum displacement achievable and slows down the time response as d/MD approaches one. It also allows reducing the overshoot by stretching back the artificial muscle toward the desired value. Figure 6 shows the time response of the SMA base artificial muscle with bias spring. The figure shows that the overshoot decreases as DD/MD increases and that the amplitude of this overshoot remains relatively large at low values of DD/MD. The reason for this is that the spring generates a force that is insufficient to counteract the actuation force of the artificial for small displacement. However, the spring force builds-up as the displacement increases while the actuation force of the AM saturates past DD/MD > 0.90.

The SMA based artificial muscle generates an activation force only when the temperature $T_{SMA} > T_A$, where T_A is the activation temperature. The first non-zero displacement for all the tests in Table 4 indicates

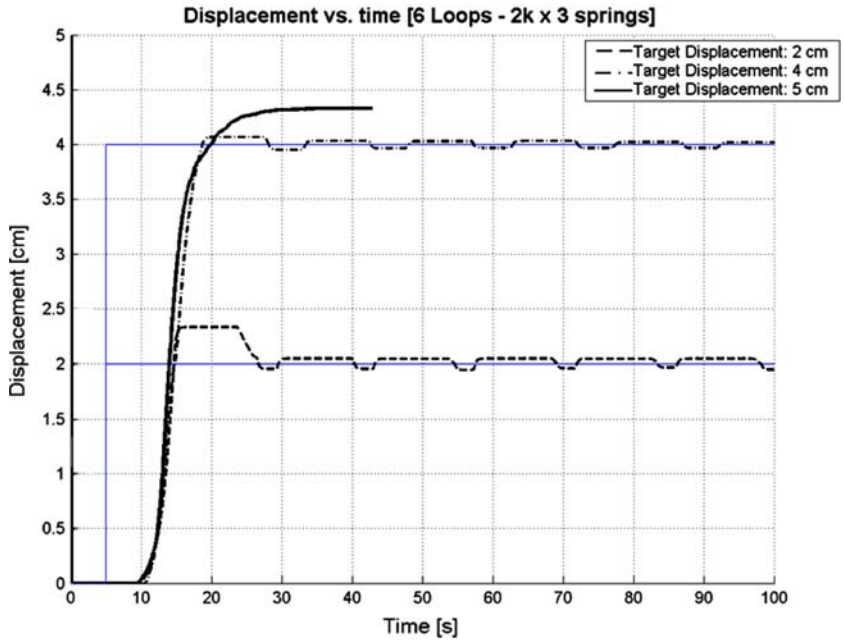

Fig. 6 Displacement of the artificial muscle with bias spring

that $T_{SMA} \approx T_A$ at $t = t_0$. Observing that the slope of the AM response for $t_o < t < t_{peak}$ is very steep, we can conclude that the actuation force is much greater than the spring force for d/MD < 0.90. When d/MD > 0.90, the spring force becomes the dominant force restricting the actuator from contracting further.

5.2 Position control of an elbow joint

In the following section, two SMA based artificial muscles are used as linear actuators in the two DOF robotic arm shown in Fig. 2. The rule-based control described in section 4 is used to activate the SMA-based artificial muscles. In order to determine the appropriate linguistic variables, several tests were conducted for different ranges as tabulated in Table 5.

Based on the results shown in Fig. 7 for a target position of 30 degrees, we can see that there are no oscillations for Test 2 and 3. After analyzing the extent at which each muscle was contracted during these tests, it was found that for an angular position approaching 27 degrees, both muscles have a DD/MD close to 1 which is consistent with the results obtained in Sect. 5.1.1 where for DD/MD > 0.9 the response has no oscillations. However, test 1 exhibits relatively large oscillations with amplitudes of up to 5 degrees, while its target position remains the same as for test 2 and 3. The reason is that the fuzzy controller will naturally try to settle at the limit between the *Positive Small* and *Zero* regions. This limit corresponds to a position of 27.5 degrees and 29.5 degrees for test 2 and 3 respectively, putting them into a situation where DD/MD $\approx$ 1. However, this limit is equal to 24.5 in the case of test 1, resulting in an ''effective target position'' corresponding to a DD/MD < 1 for which oscillations are not damped. Hence, we could state that test 1 succeeds in reaching the ''effective target position'' (i.e. the lower limit value of the *Zero* region), and oscillates around it. Analyzing the activation sequence of Fig. 8, we can

Table 4 Experimental results—Step Input

Test no.	Set-point	Δt_o	Δt_r	Δt_p	Δt_h	$t_{peak} - t_r$	PO (cm)	DD/MD
5	2	5	10	9	3	1	16 (0.33)	0.46
6	4	4	13.5	8	5.7	0.9	1.2 (0.048)	0.93
7	5	4.5	30	No oscillations		0	0	1

Table 5 Numerical representation of linguistic values for the input parameters

Test	Angular position error (e)					Target position
	Large +	Small +	Zero	Small −	Large −	
1	[10.5, ∞ [	[5.5, 10.5[	[−5.5, 5.5[	[−10.5, −5.5[	]−∞,−10.5[	30
2	[10.5, ∞ [	[2.5,10.5[	[−2.5, 2.5[	[−10.5,−2.5[	]−∞,−10.5[	30
3	[5.5, ∞ [	[0.5, 5.5[	[−0.5,0.5[	[−5.5,−0.5[	]−∞,−5.5[	30
4	[1.5, ∞ [	[0.5, 1.5[	[−0.5,0.5[	[−1.5,−0.5[	]−∞,−1.5[	20
5	[10.5, ∞ [	[0.5,10.5[	[−0.5,0.5[	[−10.5,−0.5[	]−∞,−10.5[	20
6	[5.5, ∞ [	[0.5,5.5[	[−0.5,0.5[	[−5.5,−0.5[	]−∞,−5.5[	20
7	Bang–Bang Controller					20
Tests	Angular velocity (*de*/*dt*)					
	Large +	Small +	Zero	Small −	Large −	
All	[10.5, ∞ [	[5.5, 10.5[	[−5.5, 5.5[	[−10.5,−5.5[	]−∞,−10.5[	

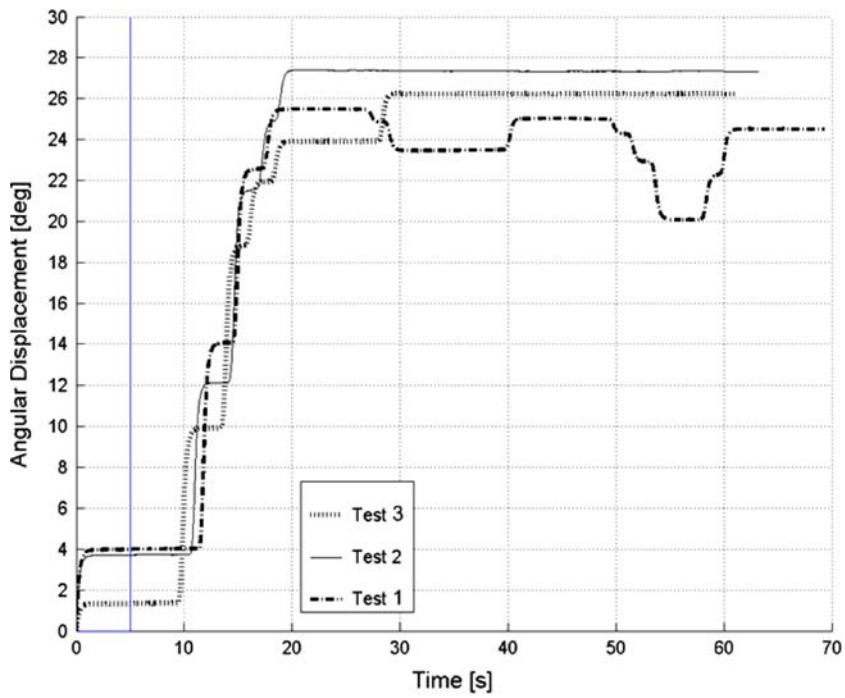

Fig. 7 Angular position of the elbow joint (Target position = 30°)

see two peaks at t = 10 s and t = 11 s for tests 2 and 3. These peaks occur when one of the two muscles are turned off in the middle of the arm motion and they are caused by the controller when it detects an angular velocity corresponding to a *Positive Large* motion. Putting to contribution the momentum of the arm in motion, the rules are designed to minimize the amount of energy spent by shutting off one muscle when the arm is already moving at a high velocity toward the desired position. The same peak can be observed at t = 15 s and 14 s for test 2 and 3 respectively, as well as t = 12 and 15 s for test 1. As previously discussed, the steady state response of test 2 and 3 ends-up in the *Positive Small* region at t = 19 s for test 2 and t = 28 s for test 3. Besides the fact that the system first reaches this region at different times (t = 15 s for test 2 and t = 27 s for test 3), we can see that in both cases it ends-up with alternating activation, corresponding to the state {e; de/dt} = {*Positive Small* ; *Zero*}. In contrast, the

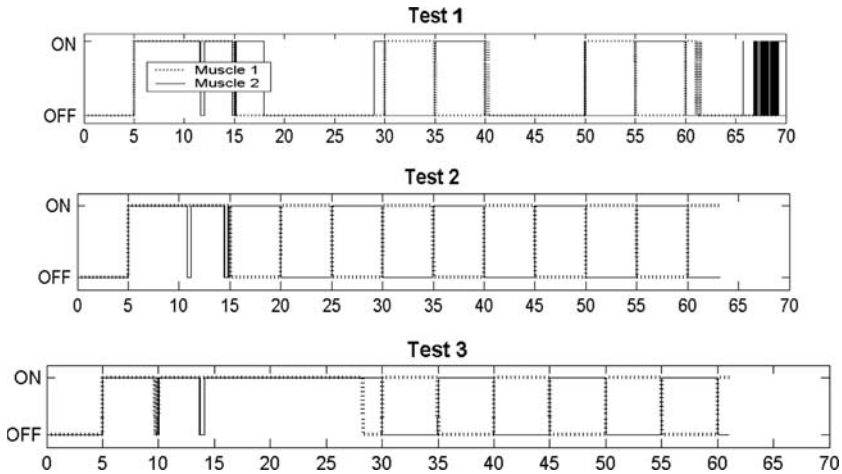

Fig. 8 Muscular activation sequence (Target Position 30°)

system in test 1 oscillates between two states once it has reached the effective target position. These states are {*Zero* ; *Zero*} and {*Positive Small* ; *Zero*} which correspond to the activation schemes ''*all off*'' and ''alternate''. The high frequency oscillations for the muscular activation of test 1 (at t > 67 s) are due to the system being exactly at the limit between the *Positive Small* and *Zero* regions for the angular position. Numerical errors inherent to the sensors-DAC equipment create very small perturbation that switches the state of the system directly from *Zero* to *Positive Small* and vice versa. As a result, muscle activation switches between ''*all off*'' and ''alternate'' at the same frequency as the numerical error switching between *Positive Small* and *Zero*. This problem should be addressed in future work. In order to make sure that the muscles were operating within their working range, the target value for the subsequent tests was set to 20 degrees. The reference test 7 that uses the Bang–Bang controller was also performed for this target position.

As for test 1, tests 4, 5 and 6 have a DD/MD < 1, implying that the SMA artificial muscles will show an oscillatory response and any damping observed in the overall behaviour is caused solely by the controller. Based on the previous observation that the controller will always attempt to reach the effective target position rather than the actual target position (the difference between the two defining the minimum steady state error), the range of the *Zero* region was set to a minimum of [−0.5; 0.5] degrees for all tests. In order to avoid the large oscillations occurring in test 1, the *Positive* and *Negative Small* regions were limited to a very small range [0.5; 1.5] in test 4. Results showed that the large oscillations remained. Trying the opposite extreme, the range was modified to [−0.5; 10.5] in test 5. Since the range was similar to the one used for test 1, the large oscillating response of test 5 confirmed the damping effect of the *Positive* and *Negative Small* regions. Modifying these regions to an intermediate range of [0.5; 5.5], test 6 shows some overshoot at the first stage of the time response and no further oscillations. Hence, the set of ranges used in test 6 were selected as the final setting for the rule-based controller. Comparing the response of test 6 with the reference response of the Bang–Bang controller in test 7, we can see that the first one has a smaller steady state error as well as a smaller initial overshoot. Moreover, test 6 doesn't have any oscillations, while test 7 shows relatively large ones. Thus, the rule-based controller is superior to the Bang–Bang controller. Observing the muscular activation responses, we can see that the large oscillations of test 4 correspond to a very small use of the alternating activation scheme. The reason is that the very short range of the *Positive Small* region (for which the activation scheme is mainly an alternating activation) doesn't give enough time for the actuator to slow down its contraction (by deactivating one of the two muscles). Thus, the system can't stabilize in the neighborhood of the desired position. In the case of test 6, the system has the time to slow down its motion when entering the *Positive Small* region as the plateau at t = 6 s to t = 9 s shows in Fig. 9. Passing through an overshoot of 3.3%, the system's angular position settles at 19.2 degrees. The key to the non-oscillatory response is that the steady state value is slightly lower than *Zero* region, making the system

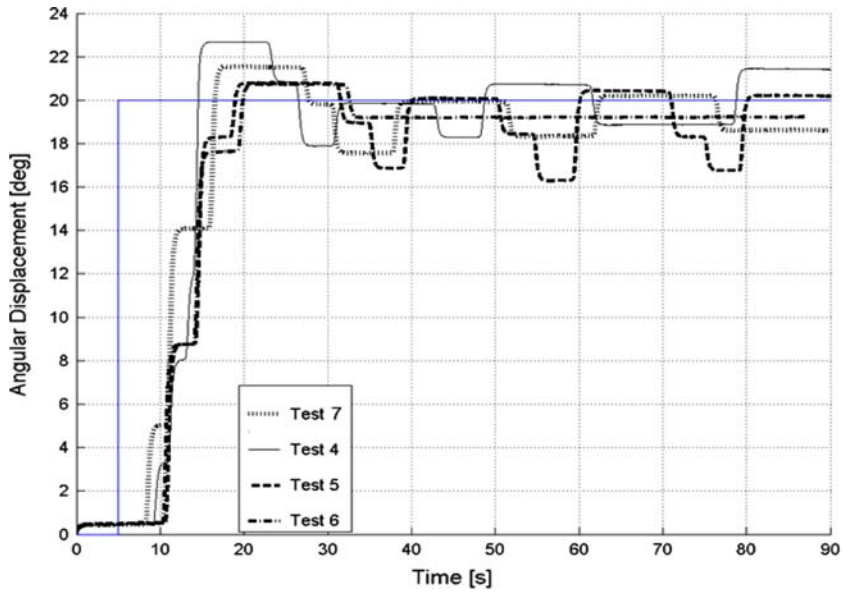

Fig. 9 Angular position of the elbow joint (Target position = 20°)

operate in an alternating actuation scheme that provides just the right amount of force to keep the position constant. If the actuation force was to be slightly higher, the system would enter into the *Zero*-region and the AM activity would die down until the position drops back in the *Positive Small* region. If the angular velocity is already high at the point of transition from *Zero* to *Positive Small* (i.e. the SMA temperature had the time to drop below the phase transition temperature), the actuation force necessary to avoid a change in the angular position will not be generated fast enough and the system will undershoot, ultimately creating oscillations around the *Zero-Positive Small* limit value as the process goes on. Thus, it is imperative not to allow the AM to cool down below the phase transition temperature. This condition can be satisfied by making the *Zero* region equal to the angular position measured when the SMA drops from its operating temperature T_{SMA} and the phase transition temperature. The interval [−0.5; 0.5] seems to be an appropriate range based on the results of this work (Fig. 10).

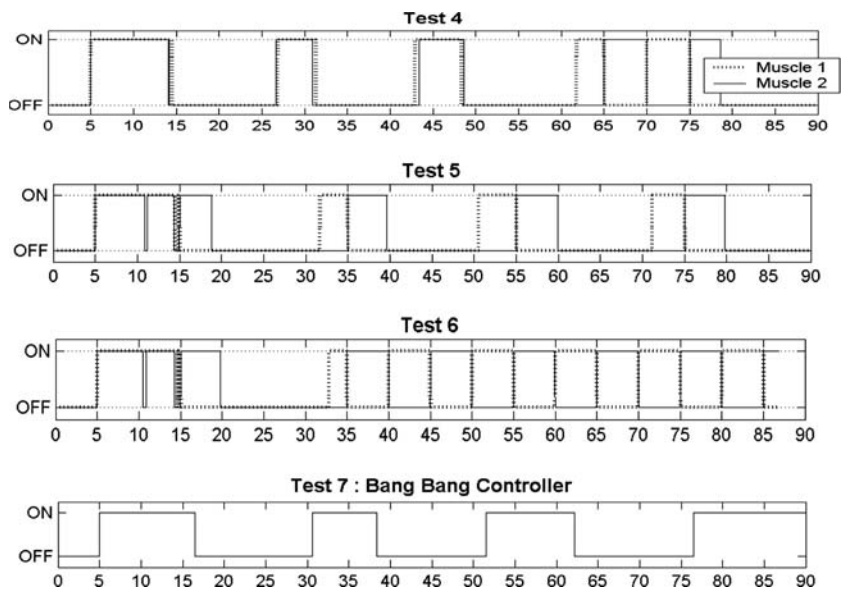

Fig. 10 Muscular activation sequence (Target Position 20°)

6 Conclusions

This paper presented an experimental study on the control of a two DOF robotic arm driven by shape memory alloy (SMA) wires. The overall strain of the SMA wire was increased from 4% when they are used as a straight wire to about 40% when the wire is arranged in the Fig. 8 shape shown in Fig. 1. Experimental results have shown that the proposed configuration increases the overall strain without compromising the recovery force. A biologically inspired control strategy using a rule-base concept was developed and tested using the two DOF robotic arm. In order to move the arm, two wires were used to represent the brachioradialis and the biceps in an elbow joint. The proposed controller activates each of the wires using a pre-defined rule base along with the angular position error and its first time derivative. Experimental results for this real-time controller showed enhanced performances over conventional Bang–Bang controller.

Appendix A

The SMA based muscles used in this study were prepared from 0.381mm (0.015in.) diameter Flexinol® wire from Dynalloy Inc. (Costa Mesa, CA).

Table A1 Model parameters for Flexinol® wire tests

Parameter	Low temp	High temp
Effective martensite start temperature, M_s [K]	328	328
Effective austenite start temperature, A_s [K]	351	351
Transformation Entropy Coefficient, s [Mpa K^{-1}]	2.78	3.72
Transformation Strain, $\varepsilon_{tr,max}$	0.06	0.07
Reorientation Stress, σ^{re} [MPa]	162.3	398.8
Activation Energy Kinetics Parameter, G	0.458	0.196
Friction kinetics parameter, c	1.115	0.016
Transformation flow kinetics parameter, n	6.543	7.235
Reverse-MT[!] interaction kinetics parameter, m	2.062	1
Forward-MT interaction kinetics parameter, l	1	1

[!] MT, martensitic transformation

Table A2 Maximum strain achieved by four-loop actuator

Load (g)	Maximum contractile strain (%)
257	31.6
471	21.3
624	15.9

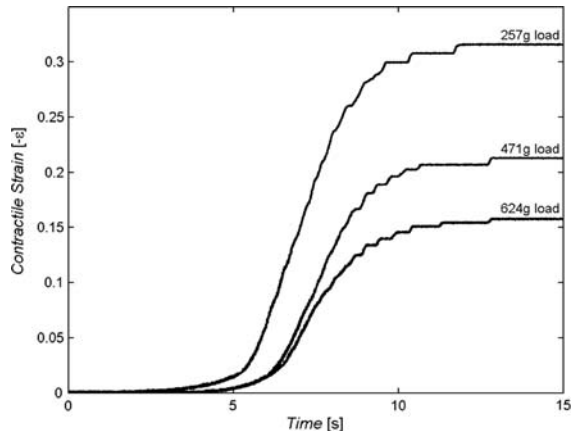

Fig. A1 Strain response at various loads for a four-loop actuator

References

Bar-Cohen, Y., Xue, T., Shahinpoor, M., Simpson, J., Smith, J.: Flexible, ''Low-mass Robotic Arm Actuated by Electroactive Polymers and Operated Equivalently to Human Arm and Hand.'' Robotics 98: The 3rd Conference and Exposition/Demonstration on Robotics for Challenging Environments. Albuquerque, New Mexico, 26–30 April 1998.

Barrett, R., Gross, R.S.: Super-active shape-memory alloy composites. Smart Mater. Struct. **5**(3), 255–260 (1996).

Benzaoui H., Chaillet N., Lexcellent C., Bourjault A.: Non Linear Motion and Force Control of Shape Memory Alloys Actuators. SPIE Conference on Mathematics and Control in Smart System, Newport Neach, California, March 1999.

Chou, C.P., Hannaford, B.: Measurement and modeling of artificial muscles. IEEE Trans. Robot. Automation **12**(1), 90–102 (1996).

De Laurentis, K., Mavroidis, C.: Mechanical Design of a Shape Memory Alloy Actuated Prosthetic Hand. Technol. Health Care **10**(1), 91–106 (2002).

Dormandy, J., Heeck, L., Vig, S.: Major amputations: clinical patterns and predictors. Semin. Vasc. Surg. **12**(2), 154–61 (2004).

Elahinia, M.H., Ahmadian1, M., Ashrafiuon, H.: Design of a Kalman filter for rotary shape memory alloy actuators. Smart Mater. Struct. **13**, 691–697 (2004).

Garner, L.J., Wilson, L.N., Lagoudas, D.C., Rediniotis, O.K.: Development of a shape memory alloy actuated biomimetic vehicle. Smart Mater. Struct. **9**, 673–683 (2000).

Gorbet, R.B., Russell, R.A.: A novel differential shape memory alloy actuator for position control. Robotica **13**, 423–430 (1995).

Icardi, U.: Large bending actuator made with SMA contractile wires: theory, numerical simulation, experiments. Compos. B: Eng. **32**(3), 259–267 (2001).

Jik Lee, H., Ju Lee, J.: Time delay control of a shape memory alloy actuator. Smart Mater. Struct. **13**, 227–239 (2004).

Ma, N., Song, G.: Control of shape memory alloy actuator using pulse width modulation. Smart Mater. Struct. **12**, 712–719 (2003).

Makaran, J.B., Dittmer, D.K., Buchal, R.O., MacArthur, D.B.: The SMART wrist-hand orthosis (WHO) for quadriplegic patients. J. Prosthetics Orthotics 5(3), 73–76 (1993).

McComas, A: Skeletal Muscle: Form and Function. Published by Human Kinetics (1996).

Pezzin, L.: Use and satisfaction with prosthetic limb devices and related services. Arch. Phys. Med. Rehabilit. **85**(5), 723–729 (2004).

Pfeiffer, C., De Laurentis, K., Mavroidis, C.: Shape Memory Alloy Actuated Robot Prostheses: Initial Experiments. Proc. of the 1999 IEEE International Conference on Robotics and Automation, Detroit, May 1999, 2385–2391.

Price, A., Edgerton, A., Cocaud, C., Naguib, H., Jnifene, A.: A study on the thermo-mechanical properties of shape memory alloys based actuators used in artificial muscles. J. Intell. Mater. Syst. Struct. **18**, 11–18 (2007).

Song, G., Chaudhry, V., Batur, C.: Precision tracking control of shape memory alloy actuators using neural networks and a sliding-mode based robust controller. Smart Mater. Struct. **12**, 223–231 (2003).

Troisfontaine, N., Bidaud, Ph., Dario, P.: Control Experiments on two SMA based micro-actuators. Fifth International Symposium on Experimental Robotics (ISER), Barcelona, Spain, 15–18 June 1997.

Tu, K.-Y., Lee, T.-T., Wang, C.-H., Chang, C.-A.: Design of a fuzzy walking pattern (FWP) for a shape memory alloy (SMA) biped robot. Robotica **17**, 373–382 (1999).

Webb, G.V., Kurdila, A.J., Lagoudas, D.C.: Hysteresis modeling of SMA actuators for control applications. Intell. Mater. Syst. Struct. **9** (1998).

Webb, G., Wilson, L., Lagoudas, D., Rediniotis, O.: Control of SMA actuators in dynamic environments. SPIE Conference on Mathematics and Control in Smart System, Newport Neach, California, March 1999.

van der Wijst, M.W.M., Schreurs, P.J.G., Veldpaus, F.E.: Application of computed phase transformation power to control shape memory alloy actuators. Smart Mater. Struct. **6**, 190–198 (1997).